Original article

3D printed components of microbial fuel cells: Towards monolithic microbial fuel cell fabrication using additive layer manufacturing

Jiseon You [a], Richard J. Preen [b], Larry Bull [b], John Greenman [a], Ioannis Ieropoulos [a,*]

[a] Bristol BioEnergy Centre, University of the West of England, Bristol BS16 1QY, UK
[b] Department of Computer Science and Creative Technologies, University of the West of England, Bristol BS16 1QY, UK

ABSTRACT

For practical applications of the MFC technology, the design as well as the processes of manufacturing and assembly, should be optimised for the specific target use. Another burgeoning technology, additive manufacturing (3D printing), can contribute significantly to this approach by offering a high degree of design freedom. In this study, we investigated the use of commercially available 3D printable polymer materials as the MFC membrane and anode. The best performing membrane material, Gel-Lay, produced a maximum power of $240 \pm 11\ \mu W$, which was 1.4-fold higher than the control CEM with P_{MAX} of $177 \pm 29\ \mu W$. Peak power values of Gel-Lay (133.8–184.6 μW) during fed-batch cycles were also higher than the control (133.4–160.5 μW). In terms of material cost, the tested membranes were slightly higher than the control CEM, primarily due to the small purchased quantity. Finally, the first 3D printable polymer anode, a conductive PLA material, showed significant potential as a low-cost and easy to fabricate MFC anode, producing a stable level of power output, despite poor conductivity and relatively small surface area per unit volume. These results demonstrate the practicality of monolithic MFC fabrication with individually optimised components at relatively low cost.

Introduction

With ever-increasing demand for sustainable energy and clean water, microbial fuel cell (MFC) technology has been receiving increasing attention. Two decades of intensive research and collective effort exerted from various angles, have resulted in significant improvements in the technology, both in terms of power output and level of understanding. The power output of a single MFC unit has increased almost exponentially and some researchers have claimed that, at least at laboratory-scale, the achievable current density of MFCs is already sufficient for practical applications [1]. The use of MFCs has also resulted in new knowledge of bacterial metal ion reduction (e.g., Fe(III) oxides), electron transfer mechanisms of anodophiles, and conductive biofilms [2–4]. A wide variety of potential applications of MFC technology has been suggested, including electricity generation, wastewater treatment, hydrogen production, and bio-sensing [5–10]. Further applications, such as pollution treatment and resource recovery have also been reported [11,12]. With this development and effort, there have been some successful examples of practical applications. Two

robots, Chew-Chew and EcoBot I, both powered by MFCs were developed in the early 2000s [13,14]. Biochemical oxygen demand (BOD) measuring sensors using MFCs are commercially available (HABS2000, KORBI) and benthic MFCs as on-site power sources for sensors and acoustic communication devices have also been reported [15]. More recently, charging a commercial mobile phone with a stack of 24 MFCs was demonstrated [5] and field trials of urinals powered by urine-fed MFCs were successfully completed [16]. The MFC technology has now reached an exciting juncture, showing great potential for practical and commercial applications.

In order to realise such applications at larger scale however, it is necessary to improve system efficiency in terms of performance levels, manufacturing and running costs, and stability along with longevity. This can be achieved through the optimisation of the system design for individual MFCs and whole stack systems, as well as the processes of manufacturing and assembly. Depending on specific applications, different system designs are required. Manufacturing and assembly processes can be significantly improved through the design process. For example, the functionality of neighbouring parts can often be consolidated, thereby reducing or eliminating the need for assembly (i.e., monolithic design.) This could allow for cost-effective, consistent and stable performance with minimum human-error as well as performance improvements.

* Corresponding author at: Bristol BioEnergy Centre, Bristol Robotics Laboratory, University of the West of England, T-Block, Frenchay Campus, Bristol BS16 1QY, UK.
E-mail address: ioannis.ieropoulos@brl.ac.uk (I. Ieropoulos).

Applications of additive manufacturing (AM), also known as 3D printing, have been expanding rapidly, including industrial prototype printing, lightweight machines [17], medical implants [18,19] and the arts [20]. Compared with other traditional manufacturing methods involving subtractive or moulding/casting processes, AM has a higher degree of design freedom, making it possible to rapidly prototype complex structures with novel materials, which could not have previously been constructed using traditional machining.

AM technology can expand the range of novel MFC architectures [21] and anode electrodes [22]. We have previously shown the potential of 3D printed MFC membranes using the polymer, Tangoplus acrylate photopolymer resin [23]. It is therefore possible to build a complete MFC from different materials using 3D printing. This enables the optimisation of individual MFC components and makes reactor design easier and more efficient, which in turn leads to functional improvement of the system. AM technology can also make the assembly of MFCs easier and quicker [24], thus saving time and reducing human error. This is particularly important for MFC system scale-up through building stacks of multiple MFC units. It also facilitates the construction of a functional system at a relatively low price.

Although the previous study [23] testing Tangoplus membrane showed the potential of 3D printed membranes, its power generating performance (0.92 μW peak power as the highest value of a batch feeding cycle under impedance matching conditions) was much lower than that of a conventional cation exchange membrane (11.39 μW). Another study [22] demonstrated great potential for a 3D printed metal anode, however metal 3D printing is currently very costly and the tested material, $AlSi_{10}Mg$ alloy, was prone to corrosion (although not significant) for the tested period of 5 months. Therefore research should continue to seek low cost, but well performing 3D printable materials for MFC components.

In this study, three 3D printed membranes in porous filaments and one anode material made of conductive PLA filament were compared with a conventional cation exchange membrane and a plain carbon veil anode. The specific objectives of this study were: (1) to compare the performance of 3D printable materials for MFC membranes and anodes with conventional materials, (2) to investigate the strengths and limitations of each material, and (3) to demonstrate the practicality of monolithic MFC fabrication.

Materials and methods

Fused deposition modelling (FDM)

Three commercially available membrane materials and one anode material were chosen to be compared with the previously used membrane and anode materials [23]. A desktop 3D printer (Replicator 2, MakerBot) was used to print the tested membranes and anode (see Fig. 1).

For membrane comparison, three Poro-Lay series filaments, Lay-Fomm 60, Lay-Felt and Gel-Lay (Formfutura, Netherlands) were selected. These filaments consist of rubber-elastomeric polymers (functional components) and part polyvinyl acetate (PVA, soluble binder) which dissolves in water. The functional component (backbone material) which gives each filament its unique features is polyurethane for Lay-fomm and polyamide for Gel-Lay respectively. The functional component of Lay-Felt is unknown as this information is not publicly available. The thickness of the control cation exchange membrane (CEM, CMI-7000, Membrane International, USA) was 0.45 mm, whereas the 3D printed membranes had a 2 mm thickness in order to reduce leakage from the anodic chamber. To dissolve the soluble components of the membrane materials, all printed membranes were submerged in water for 3 days and the water was replaced twice a day, as per the manufacturer's instructions.

For the anode material comparison, a conductive polylactic acid (PLA) based filament (ProtoPlant, USA) was printed in the shape of a rectangular mesh for higher surface area. The geometric size of the 3D printed anode was similar to the control plain carbon veil anode after being folded. Computer aided designs of the printed membrane and anode are shown in Fig. 2 and the printing process settings for both the membranes and the anodes are presented in Table 1.

MFC design and operation

Analytical style, cuboid, single-chamber MFCs (with an anodic chamber volume of 25 mL as previously described [23]) were used in this study. As a control anode material, plain carbon fibre veil electrodes (carbon loading: 20 g m^{-2}, PRF Composite Materials, UK) 270 cm^2 in area (width: 30 cm, length: 9 cm) were used. The sheet was folded several times into a rectangular shape in order to fit in the anodic chamber. The projected area of the folded anode material was 8.4 cm^2. Each tested membrane with an area of 30 cm^2 (width: 6 cm, length: 5 cm, projected surface area: 25 cm^2) was placed between the anode and cathode frames. A commercially available cation exchange membrane (CEM) was used as a control for the membrane comparison. A hot-pressed activated carbon cathode electrode, prepared as previously described [25,26] with a total surface area of 8.8 cm^2 (width: 2.5 cm, length: 3.5 cm) was placed onto the membrane as the cathode electrode.

The MFCs were inoculated with sewage sludge (Wessex Water, Saltford, UK) enriched with 1% tryptone and 0.5% yeast extract for a week. Subsequently, 10 mL of synthetic wastewater [27] was provided as the feedstock every 3–4 days unless otherwise stated. The synthetic wastewater was prepared by adding the following to 1 L of distilled water: 0.270 g $(NH_4)_2SO_4$, 0.060 g $MgSO_4 \cdot 7H_2O$, 0.006 g $MnSO_4 \cdot H_2O$, 0.13 g $NaHCO_3$, 0.003 g $FeCl_3 \cdot 6H_2O$, 0.006 g $CaCl_2 \cdot 2H_2O$, 0.006 g K_2SO_4. Acetate was used as the carbon energy source at a concentration of 20 mM. The conductivity and pH of the synthetic wastewater were 3.0 ± 0.4 mS cm^{-1} and 7.3 ± 0.2, respectively. Initially, 9 kΩ external resistors were connected to all MFCs, and subsequently, the resistance value was varied in order to match the internal resistance value of each MFC following polarisation measurements. After week 5, when all MFCs were giving a reproducible output, 700 Ω was connected to all MFCs apart from the MFCs with 3D printed anodes, whose load was 3 kΩ. All experiments were carried out in a temperature controlled environment, at 22 ± 2 °C. The experimental parameters for the different materials are summarised in Table 2.

Analysis

Scanning electron microscopy (SEM)

Scanning electron microscopy (model name-XL30, Philips) was used to examine the structural changes in the tested membranes after treatment with water and also the structural characteristics of the tested anode surfaces. For non-biological samples (membrane materials), 0.5 cm^2 area of each material was cut and fixed on aluminium mounts using contact adhesive. In order to observe the activated structures without drying them, samples were imaged in wet conditions. For biological samples (anode materials), the samples were fixed in 4% glutaraldehyde in phosphate-buffered saline (PBS).

Chemical oxygen demand (COD) analysis

Samples of 2 mL volume were taken before and after each batch cycle and filter-sterilised with 0.45 μm syringe filters (Millex, UK)
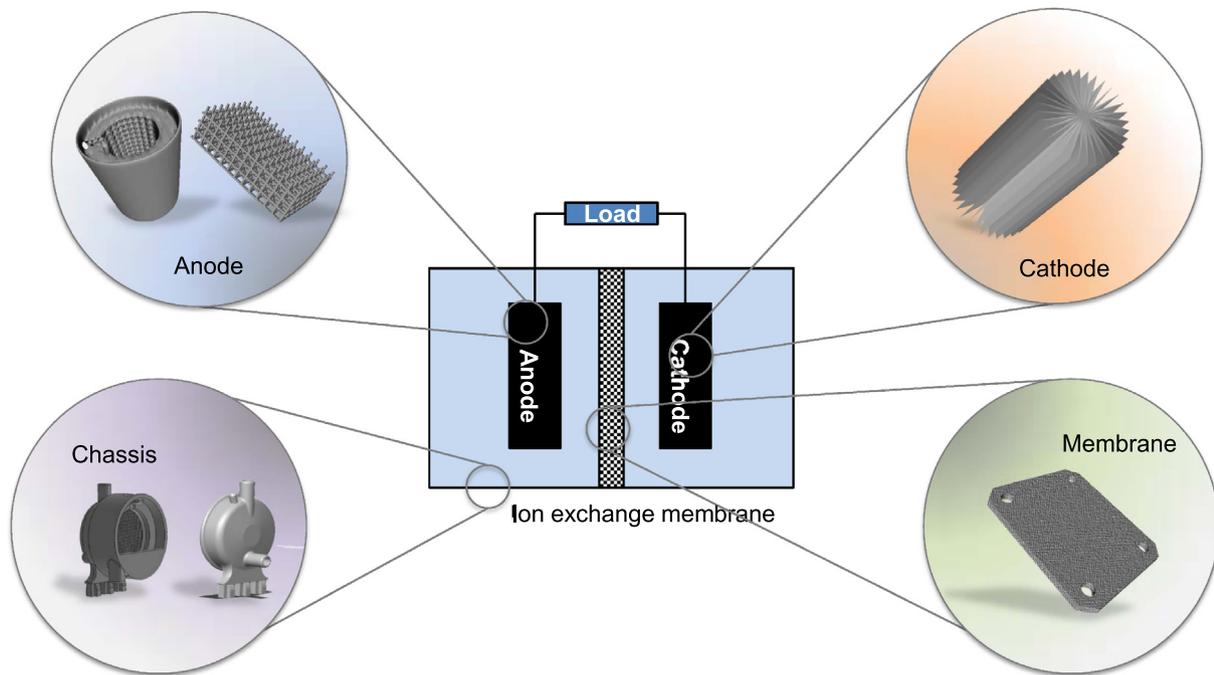
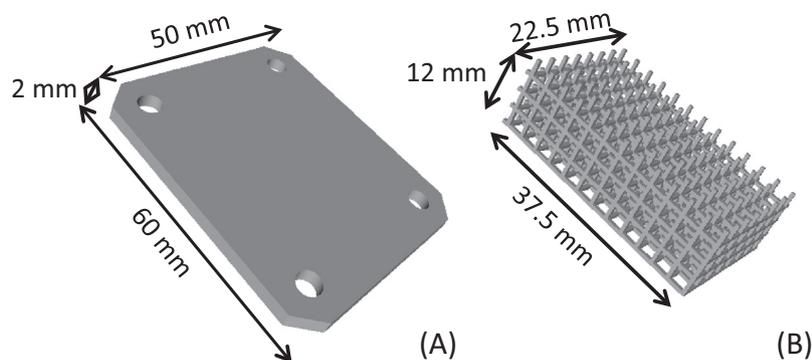**Fig. 1.** 3D printable components of a microbial fuel cell.

Fig. 2. Computer aided design drawings of the 3D printed membrane (A) and anode (B).

Table 1
3D printing process parameters for membrane and anode.

Parameters	Membrane	Anode
Object infill	10%	10%
Layer height (resolution)	0.2 mm	0.3 mm
Travel rate	150 mm s^{-1}	150 mm s^{-1}
Plastic filament diameter	1.75 mm	1.75 mm
Extrusion temperature	230 ℃	230 ℃

prior to analysis. COD was determined using the potassium dichromate oxidation method (COD MR test vials, Camlab, UK) and analysed with an MD 200 photometer (Lovibond, UK).

Four-wire resistance measurement

In order to measure the volume resistivity of the tested anode material, a 4-wire resistance measurement was carried out with a digital multimeter (M-3850D, METEX, Korea) and bench power supply (PSM-3004, GW INSTEK, Taiwan). A small sample of the 3D printed part (15 mm × 15 mm, 0.2 mm resolution, 100% in-fill) was placed between two clamps. Voltage drop between the two points, perpendicular to layers, was measured when constant current was supplied to the material from the power supply.

Polarisation measurement and Coulombic efficiency calculation

Power output of the MFCs was monitored continuously in real time in volts (V) using an ADC-24 Channel Data Logger (Pico Technology Ltd., UK). Polarisation measurements were carried out once a week, using an automated computer-controlled variable resistor system [28]. A total of 25 resistance values, starting from 39 kΩ down to 12 Ω were applied for 5 min each, after the MFCs had established steady-state open circuit voltages at the start of the experiment. Internal resistance (R_{INT}) was calculated from the power curves, at the point of maximum power production, according to Jacobi's impedance matching law (maximum power transfer theorem).

Coulombic efficiency (CE), defined as the ratio between electron moles extracted as current and the total electron moles made available from substrate oxidation [29], was calculated as follows:

$$CE = \frac{8 \int_0^t I \cdot dt}{(F \cdot V_{an} \cdot \Delta COD)} \cdot 100 \tag{1}$$

Table 2
Details of tested materials in the study.

		Control	Lay-Fomm	Gel-Lay	Lay-Felt	Conductive PLA
Anode	Material	Plain carbon veil				Conductive PLA
	Projected surface area (mm × mm)	22.5 × 37.5 (a sheet before being folded: 90 × 300)				22.5 × 37.5
	Thickness (mm)	12				12
	Volume resistivity (ohm-cm)	4.6 × 10^{-2} (measured)				3D printed parts perpendicular to layers: 44 (measured), 30 (provided by the manufacturer)
Membrane	Material	Cation exchange membrane (CMI-7000)	3D printed polymer membrane (Lay-Fomm)	3D printed polymer membrane (Gel-Lay)	3D printed polymer membrane (Lay-Felt)	Cation exchange membrane (CMI-7000)
	Composition	Polymer structure – gel polystyrene cross linked with divinylbenzene Functional group – sulphonic acid	Soluble binder – polyvinyl acetate Functional component – polyurethane,	Soluble binder – polyvinyl acetate Functional component – polyamide,	Soluble binder – polyvinyl acetate Functional component – unknown polymer	Polymer structure – gel polystyrene cross linked with divinylbenzene Functional group – sulphonic acid
	Projected surface area (mm × mm)[a]	45 × 55				
	Thickness (mm)	0.45	2 (pre-treatment) 3 (post-treatment)	2 (pre-treatment) 2.5 (post-treatment)	2 (pre-treatment) 2.5 (post-treatment)	0.45

[a] Projected surface area after subtracting area not being used due to clamping gaskets. Size of each cut membrane before assembly was 50 mm × 60 mm.

where I is the current (A), F represents Faraday's constant (96,485 C mol^{-1}), and V_{an} is anolyte volume (L). ΔCOD is equal to the difference between initial COD and final COD after a batch cycle (values in g L^{-1}).

Results

Power generating performance of 3D printed membranes

The electricity generating performance of all MFCs with tested membranes continuously increased, as the anode biofilms matured over time. The values of internal resistance calculated from weekly power curves decreased during the same period. In week 5, the MFCs with 4 types of membranes were considered to be fully mature, since they gave reproducible output in each feeding cycle and their internal resistances were consistent.

Polarisation measurements performed at the end of the 5th week are shown in Fig. 3. The open circuit voltage (OCV) of all tested membranes was similar, between 480 and 500 mV. The best performing membrane material, Gel-Lay, produced a maximum power (P_{MAX}) of 240 ± 11 µW, which was 1.4-fold higher than the control CEM with P_{MAX} of 177 ± 29 µW. The second best performing membrane material, Lay-Felt, also showed higher P_{MAX} (186 ± 3 µW) than the control. Unlike the previous two 3D printed

membranes, P_{MAX} of Lay-Fomm was lower than the control (137 ± 25 µW). MFCs with conductive PLA anodes and the same control membranes, CEMs, showed the lowest P_{MAX} of 43 ± 1 µW.

The power output of each type of membrane in week 6 is illustrated in Fig. 4. During this week the MFCs were fed 4 times in total. Unlike the usual feeding, when the previous substrate was almost completely depleted and power output dropped below 5 µW, there was an additional feeding on day 42, following the 2nd feeding (see Fig. 4, section B), in order to investigate the effect of feeding before complete depletion of the previous feedstock (replete conditions). The power output of the control, Gel-Lay and Lay-felt membranes increased rapidly after the 1st and 2nd feedings, then dropped sharply as the provided substrate became depleted. The peak power of the Lay-Fomm membrane was lower than that of the others, which is consistent with the polarisation results. However the power output from the Lay-Fomm stayed fairly stable for at least a day, then rapidly decreased. At the third feeding (section B), the peak power values of the tested membranes – except Lay-Fomm – were lower, but the sharp drop in output happened later than the first feeding since there was utilisable substrate still left from the previous feeding, implying that stable power output can be obtained under continuous feeding conditions. In terms of peak power, the 3D printed membranes showed comparable performance with the control CEM. The peak
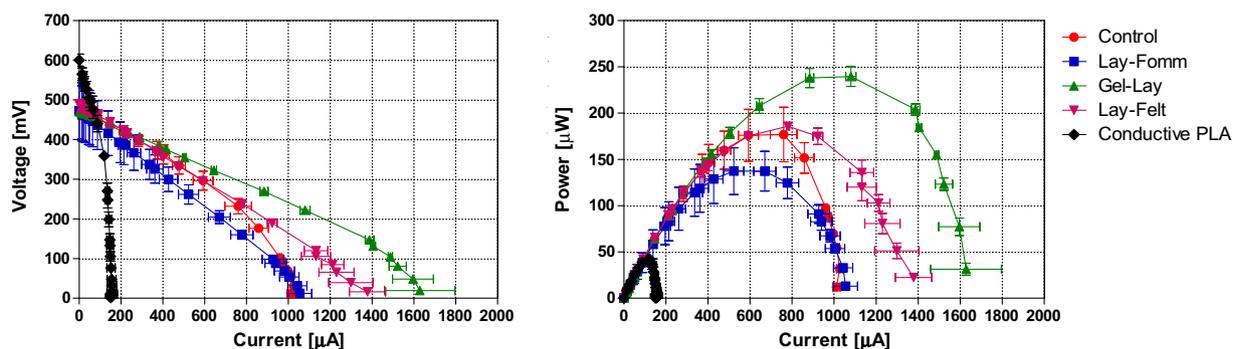

Fig. 3. Polarisation (left) and power (right) curves of tested MFCs at the end of week 5 of the experiment.
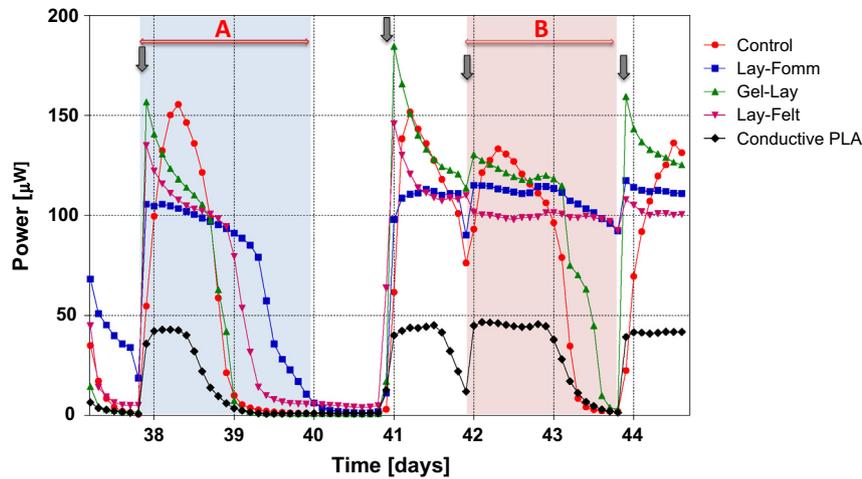
Fig. 4. Power output produced from MFCs with different membrane and anode materials between days 37–45. Grey arrows indicate when new feedstock was supplied.

power of the control for 4 fed-batch cycles was approximately 133.4–160.5 µW. The Gel-Lay membrane showed the highest peak power values of all tested membranes with a range of 133.8–184.6 µW during the same time, followed by Lay-Felt (107.0–155.9 µW) and Lay-Fomm (106.0–120.2 µW).

Although Lay-Felt and Lay-Fomm had lower peak power values compared with the control, more power was generated for the same period of one batch cycle when comparing total power generation calculated by area under the curve (AUC). Since AUC is the integral of a measurable effect or phenomenon, this can represent indirectly the total amount of power produced for a certain time period. Table 3 shows the area under the curve (AUC) of each membrane during the first and third feeding sessions (section A and section B in Fig. 4). Section A represents the condition when all of the previously provided substrates were exhausted, whereas section B represents semi-continuous feeding condition, where an additional feedstock was supplied before the previous feedstock was depleted completely. All three 3D printed membranes produced more power than the control CEM from the same amount of feedstock. This holds true especially for Lay-Fomm, which showed stable power generation and produced the highest power output of all. In section B, peak power values of all test membranes decreased, but showed a more stable output for a longer period. AUC of each membrane during this section showed the same pattern as section A, even though the output of Lay-Fomm and Lay-Felt still did not decrease to the base line at the end of section B.

Coulombic efficiency (CE) of each membrane for section A was slightly different to the AUC results; 46% (control), 57% (Lay-Fomm), 34% (Gel-Lay) and 44% (Lay-Felt).

Material morphology of 3D printed membranes

Once printed, all the membranes were solid and rigid. Rinsing off the soluble binder component with water left only the functional components, which are flexible. Compared with Gel-Lay and Lay-Fomm, Lay-Felt was stiffer and less flexible. Fig. 5 shows the structural changes of each 3D printed membrane after

treatment with water for 3 days before use. All the materials became porous although the final structures were different, depending on their functional components. It was also observed that the extent of porosity was irregular throughout the same material. Water treatment also altered the thickness of each membrane differently, although they were initially printed at the same thickness of 2 mm. The thicknesses of each membrane after treatment were: 2.5 mm, 2.5 mm and 3 mm for Lay-Felt, Gel-Lay and Lay-Fomm, respectively. As shown in these microscopic images, Lay-Felt became fibrous after treatment.

Different amounts of anolyte loss were also observed in the MFCs with the tested membranes during the same period. After one batch cycle (section A in Fig. 4), 1 mL, 3 mL and 0.5 mL of anolyte was lost from Lay-Felt, Gel-Lay and Lay-Fomm respectively, while 0.5 mL of anolyte was lost from the CEM MFCs.

Power generating performance of 3D printed anode

Similar to the previous experiments, the electricity generating performance of the 3D printed anode MFCs increased continuously, while the internal resistance value (calculated from power curves) decreased. The same control MFCs that had been used for membrane comparison, were also used as controls for anode comparison, since all the parts were identical except the anodes.

The polarisation data in Fig. 3, showed that the starting open circuit voltage of the conductive PLA anode-based MFC was higher (around 600 mV) than the other MFCs with the experimental or control membranes (480–500 mV). Thus the anodic redox potential value of the conductive PLA anode is lower than that of the plain carbon veil anode material. This was then followed by a steep decrease in polarisation performance, with almost a vertical drop, inconsistent with typical polarisation behaviour profiles. This type of performance suggests that the MFC with this conductive anode was severely activation-loss and mass-transfer limited. This was reflected by the internal resistance, which for this conductive PLA anode material (3 kΩ) was much higher than that of the control. Consequently the P_{MAX} of the 3D printed anode was lower than

Table 3
Area under the curve of two feeding sections.

Section	Control	Lay-Fomm	Gel-Lay	Lay-Felt
A	122.7 ± 5.2	168.4 ± 24.4	127.9 ± 54.6	151.9 ± 38.7
B	145.0 ± 9.1	210.4 ± 35.2	176.8 ± 72.0	191.9 ± 78.4

(A) Lay-Felt: material surface pre-treatment

(B) Lay-Felt: material surface post-treatment

(C) Gel-Lay: material surface pre-treatment

(D) Gel-Lay: material surface post-treatment

(E) Lay-Fomm: material surface pre-treatment
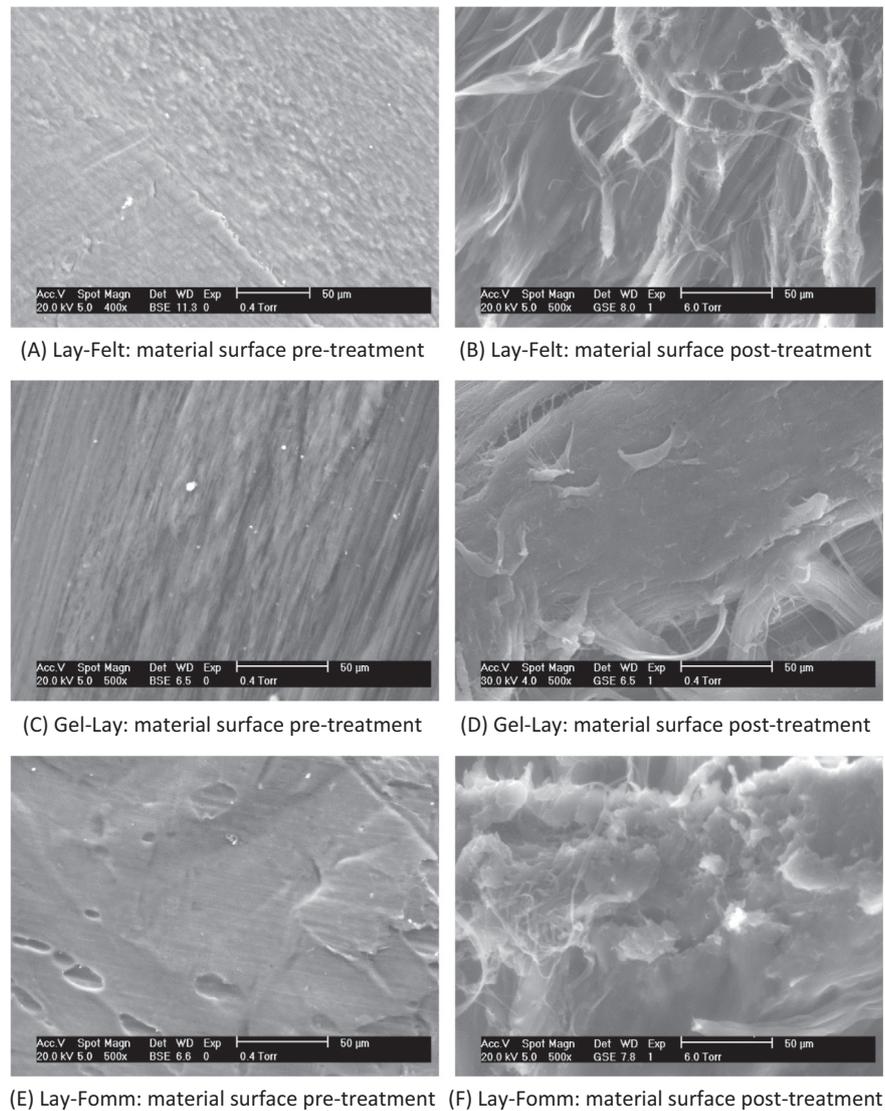
(F) Lay-Fomm: material surface post-treatment

Fig. 5. Membrane material before and after activation treatment, scale bar: 50 μm.

the control; $43 \pm 1\,\mu W$ versus $177 \pm 29\,\mu W$. Since all the other parameters, including inoculum and feedstock, were kept the same, this higher R_{INT} is assumed to be caused by the properties of the subject anode material – such as electrical conductivity, surface area – and consequent bacterial colonisation.

Once the biofilm was established on the surface of the 3D printed anode, stable and reproducible power was generated; although the peak power values of batch cycles were approximately a quarter of those of the control (Fig. 4). During one batch cycle (section A in Fig. 4), the AUC and CE of the tested anode were 35.7 and 15% respectively (compared to 122.7 AUC and 46% CE for the control).

The conductive PLA anode was printed to have the same geometry as the control plain carbon veil anode for the purposes of comparison, but it is logical to assume that the area of its surface available to anodophilic bacteria for colonisation was much smaller, with less porosity at the molecular level compared to materials such as carbon veil – as shown in Fig. 5. From the SEM images of the used anodes, biofilm established on the material surface was also observed (see Fig. 6). Since bacterial identification was not performed, it is not clear how much of this biofilm consisted of

electro-active species, but it does confirm that the conductive PLA anode material is biocompatible.

Cost of 3D printed membranes and anode

The cost of the raw materials required to produce each novel membrane and anode was slightly higher than that of using the pre-fabricated CEM and plain carbon veil materials of an equivalent size. The cost of producing one membrane in Lay-Fomm, Gel-Lay, and Lay-Felt was between € 0.58–0.60 (Formfutura), compared with € 0.30–0.56 (Membrane International) for the equivalent size of CEM material. For the same geometric anode size, € 0.24–0.29 was spent for the tested anode raw material while € 0.23–0.24 for the control. The cost of the CEM was calculated in different sizes of single sheets available from the manufacturer. The price difference between the smallest size (1.2 m × 0.5 m) and the largest size (1.2 m × 3.0 m) available was nearly double, indicating that the price for the raw materials depends greatly on production quantity. Thus the higher cost of 3D printed membrane materials, compared to the control material, would be much lower if mass-produced. Also the quantity of 3D printable materials could
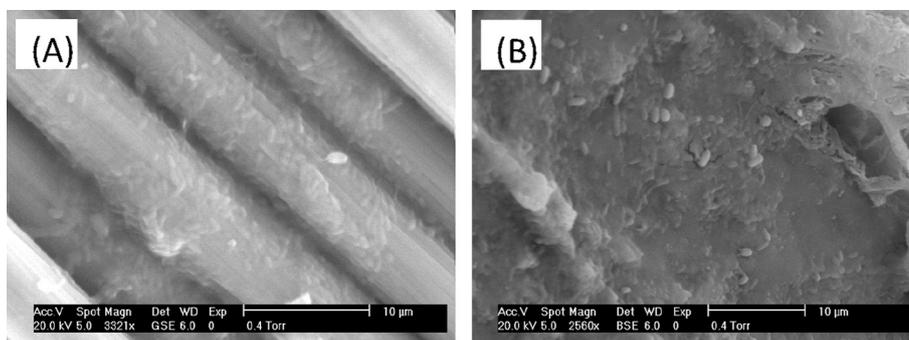
Fig. 6. Anode material surface characteristics and biofilm formation, scale bar: 10 μm; (A) plain carbon veil, (B) conductive PLA.

be reduced easily by optimising design parameters – such as thickness or shape.

Discussion

Overall, this study successfully demonstrated that with the help of material science, monolithic MFC fabrication is possible, without the need for multi-part production and costly assembly. It was also shown that this can be achieved with cost-effective and durable materials for mass production and long term operation.

Unlike ion-selective membranes, such as cation exchange membrane (CEM) or anion exchange membrane (AEM), 3D printed membranes are non-(ion) selective porous materials. Thus, the charge transfer through 3D printed membranes is facilitated by the porosity of materials. Non-selective materials have been tested in MFCs and some of them have shown excellent performance as membranes [30,31]. For these membranes, the size of pores and the level of porosity are key factors in determining their performance. Larger size pores are more favourable for proton transfer and pH splitting. They are however prone to substrate loss and oxygen permeation [32].

Anolyte loss is caused by several factors, such as anolyte evaporation, electro-osmosis or mechanical leakage due to pore size. Considering the amount of anolyte loss from MFCs with 3D printed anodes and control membrane was negligible for the same period, evaporation loss was thought to be not significant. Thus, 0.5 mL of anolyte lost from the same control membrane and Lay-Fomm was mainly due to electro-osmosis, which occurred during the electricity generating performance of MFCs since their current generation was much higher than that of the MFCs with 3D printed anodes and control membranes. A similar phenomenon was observed in a previous study reporting that the amount of catholyte accumulated was directly related to the MFC power performance [33]. For the same reason, more than 0.5 mL of anolyte loss from Lay-Felt and Gel-Lay was thought to be mainly due to leakage. It is therefore reasonable to assume that Gel-Lay has the largest pore size, followed by Lay-Felt and then Lay-Fomm. The difference in pore sizes of the tested membranes was also confirmed by the CE. The lowest CE value of Gel-Lay implies that there was a significant loss of electrons due to substrate loss and oxygen permeation, resulting from the highest porosity. However, these losses seem to be compensated by the Gel-Lay's higher P_{MAX} and peak power. If continuous-flow feeding was employed, this material could have been the best option out of all tested membranes.

On the whole, all three 3D printed membrane materials showed comparable performance with a conventional CEM, in terms of peak power and total power production. Considering design parameters such as shape, thickness and percentage of filling, which are easily manipulated, performance improvement by changing these parameters is expected – a great advantage of applying 3D printing technology to MFCs.

In the case of the 3D printable anode material, the conductive PLA anode underperformed compared with the control plain carbon veil. This low performance was thought to be mainly due to the poor conductivity of the material. Although the tested material was one of the best 3D printable conductive materials currently available on the market in terms of conductivity and ability to be printed, the volume resistivity of conductive PLA was circa 1000 times higher than the control plain carbon veil, based on measured values. Polarisation results also support this with the ohmic loss of 3D printed anode being much greater than that of the control anode material. Although the performance of currently available off-the-shelf products for the MFC anode is considerably limited due to poor conductivity, conductive polymer 3D printing could provide a better solution for a number of MFC applications requiring system scale up, where a cost-effective strategy becomes particularly important. Intensive research has been carried out [34,35] into improving the properties of 3D printable materials including electrical conductivity, it is expected that more commercially available products will appear in the foreseeable future. Areas for future work could include applying smart designs inspired by nature (biomimicry) [36] or mathematics [37] for higher surface area, incorporating printed metal parts and mechanical/chemical surface modification.

Despite this poor conductivity and surface area per unit volume, it is worth paying attention to the first 3D printable polymer electrode, which showed great potential as a low-cost and easy to build MFC anode, producing a stable and fair level of power output – as shown in Fig. 3.

In order to implement the MFC technology in the real world, system efficiency must be improved. The 3D printing technology can facilitate design optimisation of each MFC part and reactor component for specific applications, which will lead to performance improvements. Simple and easy processes of manufacturing and assembly can be taken into account from the system design process, which would again result in the improvement of system efficiency, by reducing human error in the processes and lowering system maintenance requirements. Finding low-cost materials is also very important, especially for scale up. For example, ceramic materials as membranes or chassis for MFCs have shown great performance [5,38] and 3D printable ceramic material is feasible; thus these two could be combined for 3D printable monolithic MFCs.

Conclusions

In this study, 3D printed polymer membranes and anodes were compared with conventional membrane and anode materials. 3D printed membranes showed comparable performance with a conventional cation exchange membrane, especially Gel-Lay material, which seems to be the best choice from all tested membranes due to its high power generating performance. Although the power output was lower compared with conventional plain carbon veil

material, 3D printed polymer anodes also showed a great potential when used in MFCs.

Other aspects to consider were also revealed during the study. Despite good performance, some porous filament membranes such as Gel-Lay and Lay-Felt suffered anolyte loss due to their porous structure, which resulted in a CE decrease. This could be eliminated by changing design parameters such as membrane thickness, printing resolution, or extent of filling, but this might decrease their performance. The first 3D printed polymer anode suffered from low conductivity.

The ability to 3D print MFC components enables the possibility to rapidly search and optimise novel designs and materials through iterative physical sampling, i.e., without formal models or complex simulation. The use of computational intelligence and 3D printing for such "design mining" has previously been successfully applied to the discovery of new wind turbine designs [39]. By working directly with physical prototypes there exists the potential to use subtle physical interactions in unexpected ways. Humans can be prevented from designing systems that exploit these subtle and complex characteristics through lack of understanding; however this does not prevent exploitation through a design mining approach. There is thus a real possibility that using computational intelligence, physical MFC designs manipulated through 3D printing, may allow the discovery of new physical effects, resulting in novel and more efficient MFCs.

Acknowledgements

References

[1] Hernández-Fernández FJ, Pérez de los Ríos A, Salar-García MJ, Ortiz-Martínez VM, Lozano-Blanco LJ, Godínez C, et al. Recent progress and perspectives in microbial fuel cells for bioenergy generation and wastewater treatment. Fuel Process Technol 2015;138:284–97. http://dx.doi.org/10.1016/j.fuproc.2015.05.022.

[2] Bond DR, Lovley DR. Electricity production by Geobacter sulfurreducens attached to electrodes. Appl Environ Microbiol 2003;69:1548–55.

[3] Schröder U. Anodic electron transfer mechanisms in microbial fuel cells and their energy efficiency. Phys Chem Chem Phys 2007;9:2619–29. http://dx.doi.org/10.1039/b703627m.

[4] Babauta J, Renslow R, Lewandowski Z, Beyenal H. Electrochemically active biofilms: facts and fiction. A review. Biofouling 2012;28:789–812. http://dx.doi.org/10.1080/08927014.2012.710324.

[5] Ieropoulos IA, Ledezma P, Stinchcombe A, Papaharalabos G, Melhuish C, Greenman J. Waste to real energy: the first MFC powered mobile phone. Phys. Chem. Chem. Phys. 15 (2013) 15312–6. http://dx.doi.org/10.1039/c3cp52889h.

[6] Greenman J, Gálvez A, Giusti L, Ieropoulos I. Electricity from landfill leachate using microbial fuel cells: comparison with a biological aerated filter. Enzyme Microb Technol 2009;44:112–9. http://dx.doi.org/10.1016/j.enzmictec.2008.09.012.

[7] Liu H, Liu H, Ramnarayanan R, Ramnarayanan R, Logan BE, Logan BE. Production of electricity during wastewater treatment using a single chamber microbial fuel cell. Environ Sci Technol 2004;38:2281–5. http://dx.doi.org/10.1021/es034923g.

[8] Chang IS, Jang JK, Gil GC, Kim M, Kim HJ, Cho BW, et al. Continuous determination of biochemical oxygen demand using microbial fuel cell type biosensor. Biosens Bioelectron 2004;19:607–13. http://dx.doi.org/10.1016/S0956-5663(03)00272-0.

[9] Liu H, Hu H, Chignell J, Fan Y. Microbial electrolysis: novel technology for hydrogen production from biomass. Biofuels 2010;1:129–42.

[10] Tommasi T, Chiolerio A, Crepaldi M, Demarchi D. A microbial fuel cell powering an all-digital piezoresistive wireless sensor system. Microsyst Technol 2014;20:1023–33. http://dx.doi.org/10.1007/s00542-014-2104-0.

[11] Huang L, Chai X, Cheng S, Chen G. Evaluation of carbon-based materials in tubular biocathode microbial fuel cells in terms of hexavalent chromium reduction and electricity generation. Chem Eng J 2011;166:652–61. http://dx.doi.org/10.1016/j.cej.2010.11.042.

[12] You J, Greenman J, Melhuish C, Ieropoulos I. Electricity generation and struvite recovery from human urine using microbial fuel cells. J Chem Technol Biotechnol; 2015. n/a–n/a. http://dx.doi.org/10.1002/jctb.4617.

[13] Wilkinson S. "Gastrobots" – benefits and challenges of microbial fuel cells in food powered robot applications. Auton Robots 2000;9:99–111. http://dx.doi.org/10.1023/A:1008984516499.

[14] Ieropoulos I, Greenman J, Melhuish C. Imitating metabolism: energy autonomy in biologically inspired robots. In: AISB '03, Second Int. Symp. Imitation Anim. Artifacts, Aberystwyth, Wales; 2003. p. 191–194.

[15] Gong Y, Radachowsky SE, Wolf M, Nielsen ME, Girguis PR, Reimers CE. Benthic microbial fuel cell as direct power source for an acoustic modem and seawater oxygen/temperature sensor system. Environ Sci Technol 2011;45:5047–53. http://dx.doi.org/10.1021/es104383q.

[16] Ieropoulos I, Stinchcombe A, Gajda I, Forbes S, Merino-Himenez I, Pasternak G, et al. Pee power urinal – microbial fuel cell technology field trials in the context of sanitation. Environ Sci Water Res Technol 2015. http://dx.doi.org/10.1039/C5EW00270B.

[17] Griffiths L. 3D printing for aerospace: "additive manufacturing will change the game forever". TCT Mag; 2015.

[18] Murphy SV, Atala A. 3D bioprinting of tissues and organs. Nat Biotechnol 2014;32:773–85. http://dx.doi.org/10.1038/nbt.2958.

[19] Rasperini G, Pilipchuk SP, Flanagan CL, Park CH, Pagni G, Hollister SJ, et al. 3D-printed bioresorbable scaffold for periodontal repair. J Dent Res 2015;94:153S–7S. http://dx.doi.org/10.1177/0022034515588303.

[20] Walters P, Davies K. 3D printing for artists: research and creative practice. Rapp. J Nor Print Assoc 2010;1:12–5.

[21] Ieropoulos I, Winfield J, Greenman J, Melhuish C. Small scale microbial fuel cells and different ways of reporting output. ECS Trans 2010;28:1–9.

[22] Calignano F, Tommasi T, Manfredi D, Chiolerio A. Additive manufacturing of a microbial fuel cell-a detailed study. Sci Rep 5 (2015) article no. 17373. http://dx.doi.org/10.1038/srep17373.

[23] Philamore H, Rossiter J, Walters P, Winfield J, Ieropoulos I. Cast and 3D printed ion exchange membranes for monolithic microbial fuel cell fabrication. J Power Sources 2015;289:91–9. http://dx.doi.org/10.1016/j.jpowsour.2015.04.113.

[24] Papaharalabos G, Greenman J, Melhuish C, Ieropoulos I. A novel small scale microbial fuel cell design for increased electricity generation and waste water treatment. Int J Hydrogen Energy 2015;40:4263–8. http://dx.doi.org/10.1016/j.ijhydene.2015.01.117.

[25] Santoro C, Artyushkova K, Babanova S, Atanassov P, Ieropoulos I, Grattieri M, et al. Parameters characterization and optimization of activated carbon (AC) cathodes for microbial fuel cell application. Bioresour Technol 2014;163:54–63. http://dx.doi.org/10.1016/j.biortech.2014.03.091.

[26] You J, Walter XA, Greenman J, Melhuish C, Ieropoulos I. Stability and reliability of anodic biofilms under different feedstock conditions: towards microbial fuel cell sensors. Sens Bio-Sensing Res 2015;6:43–50. http://dx.doi.org/10.1016/j.sbsr.2015.11.007.

[27] Winfield J, Ieropoulos I, Greenman J. Investigating a cascade of seven hydraulically connected microbial fuel cells. Bioresour Technol 2012;110:245–50. http://dx.doi.org/10.1016/j.biortech.2012.01.095.

[28] Degrenne N, Buret F, Allard B, Bevilacqua P. Electrical energy generation from a large number of microbial fuel cells operating at maximum power point electrical load. J Power Sources 2012;205:188–93. http://dx.doi.org/10.1016/j.jpowsour.2012.01.082.

[29] Logan BE, Hamelers B, Rozendal R, Schröder U, Keller J, Freguia S, et al. Microbial fuel cells: methodology and technology. Environ Sci Technol 2006;40:5181–92. http://dx.doi.org/10.1021/es0605016.

[30] Fan Y, Hu H, Liu H. Enhanced Coulombic efficiency and power density of air-cathode microbial fuel cells with an improved cell configuration. J Power Sources 2007;171:348–54. http://dx.doi.org/10.1016/j.jpowsour.2007.06.220.

[31] Sun J, Hu Y, Bi Z, Cao Y. Improved performance of air-cathode single-chamber microbial fuel cell for wastewater treatment using microfiltration membranes and multiple sludge inoculation. J Power Sources 2009;187:471–9. http://dx.doi.org/10.1016/j.jpowsour.2008.11.022.

[32] Li W-W, Sheng G-P, Liu X-W, Yu H-Q. Recent advances in the separators for microbial fuel cells. Bioresour Technol 2011;102:244–52. http://dx.doi.org/10.1016/j.biortech.2010.03.090.

[33] Gajda I, Greenman J, Melhuish C, Santoro C, Li B, Cristiani P, et al. Water formation at the cathode and sodium recovery using microbial fuel cells (MFCs). Sustain Energy Technol Assess 2014;7:187–94. http://dx.doi.org/10.1016/j.seta.2014.05.001.

[34] Wei X, Li D, Jiang W, Gu Z, Wang X, Zhang Z, et al. 3D printable graphene composite. Sci Rep 2015;5:11181. http://dx.doi.org/10.1038/srep11181.

[35] Postiglione G, Natale G, Griffini G, Levi M, Turri S. Conductive 3D microstructures by direct 3D printing of polymer/carbon nanotube nanocomposites via liquid deposition modeling. Compos Part A Appl Sci Manuf 2015;76:110–4. http://dx.doi.org/10.1016/j.compositesa.2015.05.014.

[36] Wegst UGK, Bai H, Saiz E, Tomsia AP, Ritchie RO. Bioinspired structural materials. Nat Mater 2014;14:23–36. http://dx.doi.org/10.1038/nmat4089.

[37] Mayama H, Tsujii K. Menger sponge-like fractal body created by a novel template method. J Chem Phys 2006;125:124706. http://dx.doi.org/10.1063/1.2336200.

[38] Walter XA, Greenman J, Ieropoulos IA. Intermittent load implementation in microbial fuel cells improves power performance. Bioresour Technol 2014;172:365–72. http://dx.doi.org/10.1016/j.biortech.2014.09.034.

[39] Preen RJ, Bull L. Toward the coevolution of novel vertical-axis wind turbines. IEEE Trans Evol Comput 2015;19:284–94. http://dx.doi.org/10.1109/TEVC.2014.2316199.